

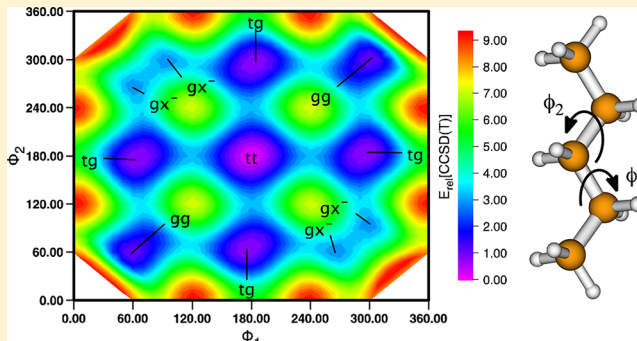
What Can We Learn about Dispersion from the Conformer Surface of *n*-Pentane?

Jan M. L. Martin*

Department of Chemistry and Center for Advanced Scientific Computing and Modeling (CASCaM), University of North Texas, Denton, Texas 76201, United States

Supporting Information

ABSTRACT: In earlier work [Gruzman, D.; Karton, A.; Martin, J. M. L. *J. Phys. Chem. A* 2009, 113, 11974], we showed that conformer energies in alkanes (and other systems) are highly dispersion-driven and that uncorrected DFT functionals fail badly at reproducing them, while simple empirical dispersion corrections tend to overcorrect. To gain greater insight into the nature of the phenomenon, we have mapped the torsional surface of *n*-pentane to 10-degree resolution at the CCSD(T)-F12 level near the basis set limit. The data obtained have been decomposed by order of perturbation theory, excitation level, and same-spin vs opposite-spin character. A large number of approximate electronic structure methods have been considered, as well as several empirical dispersion corrections. Our chief conclusions are as follows: (a) the effect of dispersion is dominated by same-spin correlation (or triplet-pair correlation, from a different perspective); (b) singlet-pair correlation is important for the surface, but qualitatively very dissimilar to the dispersion component; (c) single and double excitations beyond third order are essentially unimportant for this surface; (d) connected triple excitations do play a role but are statistically very similar to the MP2 singlet-pair correlation; (e) the form of the damping function is crucial for good performance of empirical dispersion corrections; (f) at least in the lower-energy regions, SCS-MP2 and especially MP2.5 perform very well; (g) novel spin-component scaled double hybrid functionals such as DSD-PBEP86-D2 acquit themselves very well for this problem.



1. INTRODUCTION

The IUPAC Gold Book¹ defines a conformation as “The spatial arrangement of the atoms affording distinction between stereoisomers which can be interconverted by rotations about formally single bonds”² and a conformer as “One of a set of stereoisomers, each of which is characterized by a conformation corresponding to a distinct potential energy minimum”.³ Conformers occur commonly in organic and biomolecules (which often have multiple internal rotation axes): as often many distinct conformers of such a molecule span a fairly narrow energy range, one finds that, at room or physiological temperature, the substances exist as a population mixture of conformers. Therefore, a reliable account of their properties must make allowances for these conformers—be it quantitative (e.g., conformer corrections to accurate computed thermochemical data^{4–9}) or qualitative (e.g., the use of conformer libraries for docking studies in computer-aided drug design¹⁰).

n-Alkanes are the simplest model system of this type, formally speaking. The smallest *n*-alkane with more than one conformer is of course *n*-butane, with its well-known trans and gauche conformers: four simple rules for enumerating conformers in longer alkane chains have been discovered and published.^{7,11}

In systems with intramolecular hydrogen bonds or weak hydrogen bonds (e.g., melatonin¹²), these will of course drive conformer equilibria to a large degree: obviously, they cannot be a factor in alkane conformers, and thus dispersion forces become disproportionately important.⁴ (A 1970 paper by Schleyer and co-workers may have been the first to point out the relevance of dispersion to conformer equilibria:¹³ “It is expected that favorable intramolecular van der Waals interactions, resulting from the alignment of adjacent chains in long *n*-alkanes, will allay the energetic cost of forming the gauche bonds necessary to align the chains. Cooperative folding effects, such as ‘adjacent gauche stabilization’ [...] may also be attributed to favorable intra-chain van der Waals interactions [...].”) Dispersion interactions have of course much wider importance as a crucial component of weak interactions, which themselves are fundamental to molecular recognition, supramolecular chemistry.

Recently the energetics of alkane conformers have received a fair amount of theoretical and experimental attention^{4,6,14–18} This is not just for their own sake, but also as reference data for

Received: February 8, 2013

Revised: February 28, 2013

Published: March 1, 2013

evaluation and parametrization of molecular mechanics,^{15,19} and density functional⁴ methods. (Mention should also be made of a recent study on the Raman spectrum of alkane chains with reference to imaging of biomembranes.²⁰) While it has been known for some time that DFT functionals perform below their usual par for conformer energetics,²¹ Gruzman et al. (GKM) found⁴ that conformer energy differences are a particularly sensitive test for how well a DFT method handles weak interactions, particularly dispersion which dominates the conformer energetics.^{4,13}

The main findings of GKM were: (1) conventional DFT functionals exaggerate the conformer energy spacing; (2) simple empirical dispersion corrections such as DFT-D2²² overcorrect; (3) functionals that seek to implicitly account for dispersion such as the M06 family not only overcorrect but cause tg/gg conformer inversion; (4) double-hybrid functionals, which explicitly account for some dispersion, do a much better job but still need some help from empirical dispersion corrections. The set of highly accurate *ab initio* reference data obtained by GKM has been included in the general DFT benchmark sets GMTKN24²³ and GMTKN30²⁴ by the Grimme group.

The main lacuna in GKM was that it focused on conformer equilibrium energies only, rather than on the various extrema or the entire conformer surface. Correct description of the latter may be a much more precise gauge for the correct treatment of dispersion interactions, and assist the development of more reliable models for empirical dispersion corrections. In recent years, kinetics and dynamics of conformer isomerization reactions has been the subject of experimental attention.²⁵

Very recently a paper by Tasi et al.²⁶ (TNMT) appeared that considered the topology of the *n*-pentane conformer surface, as well as considered similarity analysis of surfaces obtained at some semiempirical, DFT, and *ab initio* (HF and MP2) levels of theory, the latter using the MP2/6-31G* split-valence basis set. TNMT also identified 14 stationary points on the torsion surface (four minima, six transition states, four second-order saddle points).

In the present study, we will provide a benchmark *ab initio* torsional surface of *n*-pentane and ascertain convergence in 1-particle basis set and *n*-particle correlation treatment. We will then consider the performance of existing density functional methods and of empirical dispersion corrections. Along the way, we will obtain some insights into the nature of dispersion.

2. METHODS

All density functional calculations were carried out using Gaussian 09 releases B.01 and C.01.²⁷ CCSD(T) optimizations were likewise carried out using Gaussian 09; as the ordinary energy-only optimizer in Gaussian 09 only allows minima and transition states, the second-order saddle points were optimized through the expedient of having the “external” feature of Gaussian invoke a numerical gradient calculation with another instance of Gaussian. In this manner, the “energy-only” character of CCSD(T) was hidden from the optimization layer.²⁸ The highest level of theory at which we were able to carry out such optimizations was CCSD(T)/cc-pVTZ.

Single-point CCSD(T) calculations with larger basis sets, and optimizations of minima with same, were carried out using MOLPRO²⁹ 2010.1. The latter code was also used for single-point explicitly correlated CCSD(T)-F12b³⁰ energies.

Most calculations ran on the IBM iDataplex cluster of the Faculty of Chemistry at the Weizmann Institute of Science,

while the explicitly correlated surfaces were run, likewise using MOLPRO 2010.1, on the CASCaM cluster at the University of North Texas.

The following wave function-based electron correlation methods were considered: HF, MP2, MP3, MP4, CCSD(T), SCS-MP2,^{31,32} SOS-MP2,³³ SCS-MP3,³⁴ SCS-CCSD,³⁵ and MP2.5.³⁶

As an organizing principle for the plethora of DFT methods currently available, Perdew proposed the “Jacob’s Ladder” (using a Biblical analogy). Here Hartree theory (no exchange, no correlation) represents the “earthly vale of tears” and the hypothetical exact exchange-correlation functional Heaven. Each new type of information represents a rung on the ladder: (1) The local density approximation (LDA), which employs no other information than the density at a given point in space, occupies the first rung; (2) The second rung consists of semilocal GGAs (generalized gradient approximations), where the reduced density gradient is admitted as an information source; (3) The third rung is occupied by semilocal “meta-GGAs”, which involve either higher derivatives of the density or, containing similar information, the kinetic energy density; (4) At the fourth rung, one finds functionals dependent on the occupied orbitals, which are of course global rather than semilocal. (For a comprehensive review on orbital-dependent DFT, see ref 37). The most common examples, of course, are the well-known “hybrid functionals”, in which a fraction of “exact” Hartree–Fock-like exchange is admixed into the exchange functionals: personally, the authors have found it useful to distinguish between “incomplete fourth-rung” hybrid GGAs and “complete fourth-rung” hybrid meta-GGAs. Range-separated hybrids (RSHs) offer further grounds for finer subdivision:³⁸ they themselves can be subdivided into long-range-corrected RSHs (which have 100% HF exchange in the long-distance limit),^{39–41} and screened hybrids (which at that asymptote only have semilocal exchange).⁴² Of course, ordinary Hartree–Fock theory itself can be regarded as a special case of a fourth-rung functional (100% exact exchange, null correlation); (5) At the fifth rung are placed functionals that also involve the virtual (unoccupied) orbitals. So-called “double hybrids”, in which both HF-like exchange (that is, HF exchange in a basis of Kohn–Sham orbitals) and MP2-like correlation are admixed, are one class of fifth-rung approaches (which we will consider in this work), RPA (random phase approximation)-based approaches⁴³ are another. Straight MP2, as well as spin-component-scaled variants,³² can be considered special cases of fifth-rung functionals.

The following DFT functionals were considered: on the second rung of the “Jacob’s Ladder”,⁴⁴ BLYP⁴⁵ and PBE,⁴⁶ on the third rung, TPSS; on the fourth rung, B3LYP,^{47,45} PBE0,^{46,48} and M06;⁴⁹ and on the fifth rung, the double hybrid⁵⁰ B2GP-PLYP⁵¹ and the spin-component scaled DSD-BLYP,⁵² DSD-PBEP86,⁵³ DSD-PBEPBE,^{53b} and DSD-PBEhB95^{53b} double-hybrids. As range-separated fourth-rung functionals, we consider ω B97X and ω B97X-D of Chai and Head-Gordon.^{54,55}

Basis sets considered include: (a) The correlation consistent⁵⁶ cc-pVnZ ($n = T, Q$) basis sets and their diffuse-function-augmented variants⁵⁷ aug-cc-pVnZ ($n = T, Q$), which are optimized for correlated wave function calculations; (b) In some exploratory calculations, the Jensen⁵⁸ polarization-consistent (pc-n) basis sets which are specifically optimized for DFT applications (which is typically reflected in “softer” basis function exponents than the parallel cc-pVnZ basis sets);

Table 1. Relative Energies (kcal/mol) of the 14 Stationary Points on the *n*-Pentane Torsional Surface at Various Levels of Theory with the cc-pVTZ Basis Set^a

	CCSD(T)	B3LYP	B3LYP-D2	SCS-MP2	MP2	DSD-PBEP86-D2	DSD-PBEP86-noD	M06	M06-2X	B2GP-PLYP	B2GP-PLYP-D	PBE0	PBEOD
$\tau\tau$ SP	16.66	16.78	15.36	17.12	17.27	16.60	17.07	16.48	16.54	17.17	16.63	16.88	16.06
$\xi\tau$ SP	9.32	9.44	8.78	9.62	9.63	9.34	9.55	9.45	9.28	9.65	9.39	9.38	9.01
$\xi\xi$ SP	7.18	6.90	6.88	7.36	7.49	7.26	7.33	7.35	7.36	7.30	7.30	7.04	7.04
$\xi\xi^-$ SP	7.14	6.98	6.85	7.33	7.43	7.22	7.31	7.21	7.32	7.31	7.27	7.08	7.03
$\tau\chi$ TS	7.05	7.57	6.17	7.37	7.25	6.96	7.33	6.84	7.01	7.49	6.94	7.48	6.67
$t\tau$ TS	5.38	5.72	4.96	5.56	5.56	5.35	5.57	5.25	5.21	5.68	5.38	5.63	5.18
ξg TS	3.48	3.82	3.23	3.61	3.53	3.49	3.64	3.46	3.52	3.74	3.51	3.77	3.42
$\xi^- g$ TS	3.35	3.85	3.02	3.50	3.38	3.33	3.54	3.05	3.25	3.68	3.35	3.74	3.25
$\gamma\gamma$ TS	3.17	3.56	2.55	3.37	3.26	3.10	3.36	2.91	3.28	3.46	3.07	3.54	2.97
$\xi^- t$ TS	3.11	3.08	3.05	3.18	3.22	3.16	3.19	3.17	3.16	3.19	3.18	3.12	3.11
gx^-	2.76	3.45	2.20	2.96	2.78	2.68	2.99	2.37	2.55	3.18	2.67	3.34	2.59
gg	0.91	1.66	0.37	1.05	0.78	0.77	1.07	0.35	0.54	1.28	0.75	1.45	0.67
tg	0.58	0.91	0.34	0.65	0.55	0.53	0.66	0.47	0.55	0.74	0.52	0.82	0.49
tt	0.00	0.00	0.00	0.00	0.00	0.00	0.00	0.00	0.00	0.00	0.00	0.00	0.00
RMSD (kcal/mol)		0.41	0.58	0.22	0.24	0.07	0.21	0.25	0.16	0.32	0.09	0.33	0.25
RMSD minima		0.62	0.47	0.15	0.08	0.10	0.17	0.40	0.25	0.34	0.11	0.48	0.18

^aTS = transition state, SP = 2nd-order saddle point.

(c) The Weigend-Ahlrichs⁵⁹ def2-TZVPP and def2-QZVP basis sets, which are somewhat “amphoteric” in their applicability to wave function and DFT calculations and therefore seem like a good choice for double-hybrid DFT calculations, as well as for cross-comparisons between wave function, double-hybrid, and conventional DFT.

For comparison purposes, the *spdf* basis sets cc-pVTZ, pc-2, and def2-TZVPP can be considered to be in the same quality segment, while the *spdfg* basis sets cc-pVQZ, pc-3, and def2-QZVP likewise share a quality bracket.

The following types of empirical dispersion corrections⁶⁰ were considered: (a) Grimme’s 2006 version,²² denoted by the suffix “-D” in earlier papers and by the suffix “-D2” in the present work (to distinguish it from later versions). This model only has R^{-6} terms with fixed parameters for every atom, multiplied by a Fermi-type damping function of the form

$$f_{\text{damp}}(R_{AB}) = \frac{1}{1 + \exp(-\gamma(R_{AB}/s_R R_{0,AB} - 1))}$$

The length-scaling factor s_R is set to a fixed value of 1.1, which leaves D2 with only a single parameter s_6 for every level of theory. It is obtained by linear least-squares minimization of the error over a set of well-known weak interaction energies, generally the S22 benchmark set of Hobza and co-workers.⁶¹

(b) As part of the ω B97X-D functional,⁵⁵ the alternative correction of Chai and Head-Gordon, which resembles D2 except for a different damping function

$$f_{\text{damp}}(R_{AB}) = \frac{1}{1 + a(R_{0,AB}/R_{AB})^{-\alpha}}$$

in which they set $a = 6$ and $\alpha = 12$.

(c) Grimme’s 2010 version,⁶² denoted by the suffix “-D3” here and elsewhere. It includes R^{-8} terms as well as connectivity-dependent atomic parameters, but sets $s_6 = 1.0$ and has two parameters: the overall r^{-8} admixture coefficient s_8 and the length scaling s_R . Unlike “-D2”, published parameters for DFT-D3 cover the elements H–Pu, including the transition

metals. The Chai/Head-Gordon damping function is used, with $a = 6$ but with a slightly greater $\alpha = 14$.

(d) A minor modification of DFT-D3,⁶³ in which the cutoff function was replaced by one inspired by Becke and Johnson:⁶⁴

$$E_{\text{disp}}^{D3(\text{BJ})} = - \sum_{A>B} S_6 \frac{C_{6,AB}}{R_{AB}^6 + [f(R_{0,AB})]^6} \\ + s_8 \frac{C_{8,AB}}{R_{AB}^8 + [f(R_{0,AB})]^8}$$

with $f(R_{0,AB}) = a_1 R_{0,AB} + a_2$. This modified cutoff function does not fade to zero at short distance but to a small finite value: it has been argued⁶⁴ that this function is physically more sound and that it does not exhibit the counterintuitive behavior of increased intermonomer distances for more tightly bound species.

In addition to these “static” corrections (which use no wave function or density information, only the nuclear positions — which of necessity limits their flexibility in adapting to changing chemical environments), the Vydrov-van Voorhis (VV10)⁶⁵ “nonlocal” (NL) correction was considered, which does not rely on atomic dispersion parameters at all but instead employs a local response model that extracts all required information (except for a single short-range damping parameter) from the molecular electron density. These calculations were carried out using the implementation in ORCA 2.9.⁶⁶

In a recent review article, Klimeš and Michaelides,⁶⁷ propose a “stairway to Heaven” for dispersion corrections (by analogy to the “Jacob’s Ladder”⁴⁴ for exchange-correlation functionals). At step zero, aside from pseudopotential approaches,⁶⁸ one finds implicit treatment by parametrization of the semilocal functional: in the present work, this step is represented by the M06 family of functionals. As step one, they classify simple R^{-6} corrections with static coefficients, such as -D2 considered presently; step two is created by incorporating some degree of dependence on the chemical environment in the coefficients, such as is done in -D3 and -D3BJ, or in the more elaborate Tkatchenko-Scheffler⁶⁹ and Becke-Johnson⁶⁴ models. At step

Table 2. Backbone Torsion Angles (degree) of *n*-Pentane at a Representative Selection of Levels of Theory with the cc-pVTZ Basis Set^a

	CCSD(T)	B3LYP	B3LYP-D2	SCS-MP2	MP2	DSD-PBEP86-D2	DSD-PBEP86-noD	M06	M06-2X	B2GP-PLYP	B2GP-PLYP-D	PBE0
$\tau \times TS$	82.38	81.38	80.75	82.53	82.36	81.87	82.06	81.07	82.69	81.81	81.60	81.83
	-5.31	-4.88	-4.48	-5.42	-5.36	-5.13	-5.19	-4.89	-5.53	-5.08	-4.99	-5.04
$\xi \tau SP$	120.94	120.22	121.58	121.13	121.28	121.23	121.00	121.54	121.46	120.84	121.26	120.55
	1.33	0.79	1.63	1.32	1.60	1.54	1.45	2.36	2.12	1.27	1.49	1.29
$\xi g TS$	117.69	117.72	118.99	117.57	117.87	118.09	117.82	119.48	118.40	117.72	118.19	117.89
	69.04	69.42	67.63	69.33	69.02	68.66	68.98	69.47	68.98	69.10	68.53	68.96
$\xi \xi SP$	120.58	120.18	120.84	120.74	120.85	120.72	120.61	120.71	120.43	120.52	120.75	120.22
	120.58	120.18	120.84	120.74	120.85	120.72	120.61	120.71	120.43	120.52	120.75	120.22
$\xi^- g TS$	-122.04	-118.71	-123.33	-121.82	-122.29	-122.59	-121.71	-127.93	-124.30	-120.85	-122.49	-119.97
	67.05	66.70	66.76	67.25	66.98	67.03	66.96	69.75	67.94	66.88	66.90	66.67
$\xi \xi^- SP$	-118.97	-118.25	-119.29	-119.11	-119.03	-119.04	-118.77	-120.47	-119.01	-118.64	-119.05	-118.25
	118.97	118.25	119.29	119.11	119.03	119.04	118.77	120.47	119.01	118.64	119.05	118.25
$\xi^- T TS$	-119.73	-118.83	-119.96	-119.79	-119.89	-119.77	-119.55	-121.46	-120.22	-119.35	-119.77	-118.95
	179.00	179.28	179.20	179.02	178.85	179.02	179.01	179.48	179.60	179.08	179.04	179.16
$\gamma\gamma^- TS$	-76.13	-77.22	-76.02	-76.32	-75.95	-76.20	-76.36	-75.54	-75.09	-76.60	-76.22	-76.98
	76.13	77.22	76.02	76.32	75.95	76.20	76.36	75.54	75.09	76.60	76.22	76.98
gg	58.74	63.67	58.23	59.09	58.30	58.44	59.29	58.45	56.63	60.62	58.64	62.11
	58.74	63.67	58.23	59.09	58.30	58.44	59.29	58.45	56.63	60.62	58.64	62.11
gx-	-94.12	-90.41	-92.77	-94.50	-94.64	-93.91	-94.12	-94.41	-95.81	-93.38	-93.50	-93.00
	60.46	65.20	59.78	60.74	59.93	60.02	60.73	61.59	58.47	61.74	60.16	62.73
tg	176.22	177.33	177.43	176.14	176.18	176.70	176.66	174.88	175.37	176.91	176.90	177.29
	64.28	66.21	64.46	64.50	63.98	64.23	64.59	62.59	61.58	65.15	64.39	65.47
RMSD	2.21	0.80	0.21	0.27	0.28	0.26	1.70	1.24	0.77	0.35	1.35	

^aTorsion angles for $\tau\tau$, τt , and tt are by symmetry exactly (0,0), (0,180), and (180,180), respectively.

three, one finds long-range or “nonlocal” functionals such as VV10 (considered in this work),⁶⁵ vdwDF,⁷⁰ and vdw-DF2;⁷¹ higher steps would consider three-body terms and/or explicit long-range correlation by perturbation theory (such as the double hybrids considered in the present work) or the random phase approximation (RPA).⁴³ A full rigorous *ab initio* treatment would presumably correspond to Heaven.

3. RESULTS AND DISCUSSION

3.1. Extrema on the Potential Energy Surface. As shown by Tasi et al.,²⁶ the *n*-pentane torsion surface has 14 stationary points, namely four minima, six transition states, and four second-order saddle points. In labeling them, we use the conformational notation convention T = trans (180°), G = gauche ($\pm 60^\circ$), X = cross ($\pm 90^\circ$), γ = ($\pm 75^\circ$), ξ = skew ($\pm 120^\circ$), τ = eclipsed (0°). In cases where the two angles have the opposite sign, we indicate this by superscripts, that is, gx^- or $\xi\xi^-$.

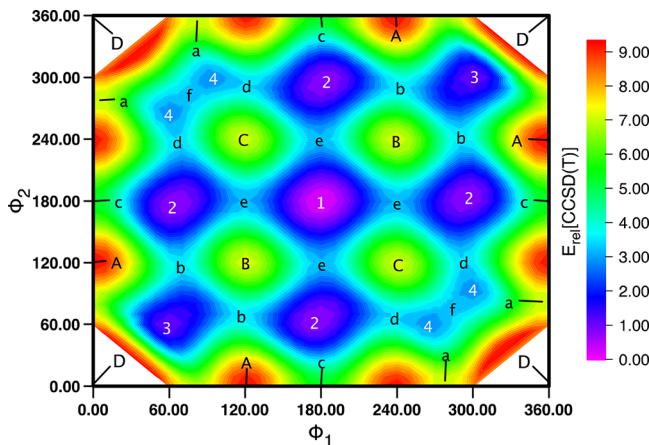
Relative energies at various levels of theory can be found in Table 1, while backbone torsion angles are given in Table 2 and molecular visualizations of all 14 extrema can be found in Figure S-1 of the Supporting Information (SI). MP2/cc-pVTZ

and SCS-MP2/cc-pVTZ harmonic frequencies, as well as Cartesian coordinates for the CCSD(T)/cc-pVTZ geometries are likewise provided in the SI, the latter both in XMol/Jmol .xyz format and as interactive Jmol objects. A graphical representation of the entire torsion surface, which may clarify the meaning of the various labels, can be seen in Figure 1.

The four second-order saddle points are located at roughly 120-degree spacing: the global maximum $\tau\tau$ (C_{2v} symmetry) at (0,0); the 4-fold degenerate $\xi\tau$ (no symmetry) at about ($\pm 120, 0$) and (0, ± 120); and two nearly equivalent doubly degenerate central maxima $\xi\xi$ (C_2 symmetry) at about ($\pm 120, \pm 120$) and $\xi\xi^-$ (C_s symmetry) at ($\pm 120, \pm 120$).

The global minimum is of course the well-known tt (C_{2v} symmetry) at (180,180); second highest in energy is the 4-fold degenerate tg (no symmetry) at about (60,180), followed by the *syn* gauche combination gg (C_2 symmetry, 2-fold degenerate) at about ($\pm 60, \pm 60$). The *anti* gauche combination, which would have been gg^- , actually is not a local minimum due to the well-known “pentane interference”, but undergoes a small splitting into degenerate gx^- structures at about ($\pm 60, \pm 90$) and ($\pm 90, \pm 60$), which is the least stable minimum.

This leaves six transition states. ξt (3.10 kcal/mol) connects tt and tg , while ξG and ξG^- (3.48 and 3.35 kcal/mol,



Minima: 1=tt (C_{2v}); 2=tg; 3=gg (C_2); 4=gx⁻.
Transition states: a=τx; b=ξg⁺; c=τt (C_s); d=ξg⁻; e=ξt; f=γγ⁻ (C_s).
Second-order saddle points: A=τξ; B=ξξ⁺ (C_2); C=ξξ⁻ (C_s); D=ττ (C_{2v}).

Figure 1. CCSD(T)/cc-pVTZ relative energy (kcal/mol) of *n*-pentane as a function of the two backbone torsion angles. Values above 9.5 kcal/mol have been clipped for better contrast elsewhere. The global $\tau\tau$ maximum at (0,0) perches 16.66 kcal/mol above the tt global minimum. White digits indicate local minima, black lowercase letters transition states, and black uppercase letters 2nd-order saddle points. Minima: 1 = tt (C_{2v}); 2 = tg; 3 = gg (C_2); 4 = gx⁻. Transition states: a = τx; b = ξg⁺; c = τt (C_s); d = ξg⁻; e = ξt; f = γγ⁻ (C_s). Second-order saddle points: A = τξ; B = ξξ⁺ (C_2); C = ξξ⁻ (C_s); D = ττ (C_{2v}).

respectively) offer pathways from tg to gg and tg to gx⁻, respectively. γγ⁻ (3.17 kcal/mol) represents just the shallow barrier between equivalent pairs of gx⁻ structures. The two final transition states $\tau\tau$ (5.38 kcal/mol, between adjacent equivalent tg⁺⁺ and tg⁻⁻) and $\tau\chi$ (7.05 kcal/mol, between adjacent equivalent gg and gx⁻) are not lowest accessible pathways: those would run via gg and tg, respectively. There is no direct pathway at all from tt to gg or gx⁻: indirect pathways run via tg. Nor is there a direct pathway from gg to G⁻⁻G⁻⁻: this transformation would proceed via tg, tt, and tg⁻⁻.

Conformer isomerization ('conformerization') pathways at the CCSD(T)/cc-pVTZ level are summarized in Table 3.

Table 3. Conformation Pathways, Transition States, and CCSD(T)/cc-pVTZ Barrier Heights (kcal/mol)

	tt	tg	gg	gx ⁻
tt	Indirectly: tt → tg → gx ⁻ → twin gx ⁻ → other tg → tt			
tg	ξt 3.106	ξt 5.381; lower indirect pathway via gg		
gg	via tg	ξg 3.479	Indirectly: gg → tg → tt → other tg → other gg	
gx ⁻	via tg	ξg ⁻ 3.350	tx 7.050; lower indirect pathway via tg	γγ ⁻ 3.170

It was pointed out earlier⁴ that the deficiencies of DFT methods express themselves not only in the relative conformer energies (see Table 1) but also in the torsional angles. For instance, at the B3LYP level one sees an error of 5 degrees in the torsion angle for the gg structure; the RMS deviation from CCSD(T) over all nontrivial torsion angles is 2.2 degrees. This latter statistic is reduced to 0.8 degrees upon addition of a D2 empirical dispersion correction (with $s_6 = 1.05$). At the PBE0

level, one finds a more respectable but still significant 1.35 degrees, which drops to 0.54 degrees with a D2 empirical dispersion correction ($s_6 = 0.60$). The M06 and M06-2X functionals, which attempt to implicitly account for dispersion, have RMSDs of 1.7 and 1.24 degrees, respectively. For comparison, straight MP2 yields 0.27 degrees, which drops further to 0.21 degrees for SCS-MP2. At similar expense, the older double-hybrid functional B2GP-PLYP yields 0.8 degrees without any dispersion correction, and 0.35 degrees with a D2 correction. The newer spin-component-scaled double hybrid DSD-PBEP86 yields essentially equivalent (and respectable) RMSDs of 0.28 and 0.26 degrees, respectively, for -D2 and dispersion-less parametrizations. (It was first found in ref 52 and again in ref 53 that the s_6 prefactor of D2 and the same-spin correlation coefficient are strongly coupled in DSD functional optimizations.) MP3, with RMSD = 0.24, performs intermediately between MP2 and SCS-MP2, while CCSD only marginally improves over SCS-MP2, at RMSD = 0.20 degrees.

For the whole surface, pointwise CCSD(T) or even CCSD or MP3 optimizations would be intractable, but SCS-MP2/cc-pVTZ is quite feasible. To what degree does this affect energetics? Comparing fully optimized CCSD(T)/cc-pVTZ with CCSD(T)/cc-pVTZ//SCS-MP2/cc-pVTZ relative energies, we found that the difference is just barely detectable on the scale of interest to us, with an RMS change of 0.003 kcal/mol and a maximum change of 0.005 kcal/mol (see Table S-1 in the SI). We thus feel justified in using the SCS-MP2/cc-pVTZ reference geometries for the remainder of the surface.

While cc-pVTZ would appear to be a good "bread and butter" basis set, at least for alkanes, the questions arise whether (a) on the one hand, is it adequate for the relative energetics, and (b) on the other hand, would a smaller basis set have yielded acceptable results?

In response to (a), we carried out explicitly correlated CCSD(T)-F12b/cc-pV{D,T}Z-F12 as well as MP2-F12/cc-pV{T,Q}Z-F12 calculations³⁰ with the aim of effectively eliminating basis set incompleteness concerns. As the (T) contribution is still calculated conventionally, an approximate F12 correction for it was obtained by scaling it with the MP2-F12/MP2 ratio, as first proposed by Marchetti and Werner.⁷² (The VnZ-F12 basis sets and matching density fitting basis sets were taken from refs 73 and 74, respectively, while the geminal exponents recommended in ref 73 were employed.) The RMSD between CCSD(T)-F12b/cc-pV{D,T}Z and CCSD(T)-F12b/cc-pV{D,T}Z was found to be just 0.005 kcal/mol (cf. Table S-1 in the SI). The difference between MP2-F12/cc-pVTZ-F12 and MP2-F12/cc-pVQZ-F12 was found to be even smaller (vide infra). We can thus assume that CCSD(T)-F12b/cc-pVTZ-F12 is adequately close to the basis set limit for our purposes.

The RMSD difference with these latter values of CCSD(T)/cc-pVTZ is 0.031 kcal/mol, which drops to 0.017 kcal/mol with the aug-cc-pVTZ and 0.008 kcal/mol with the cc-pVQZ basis set. Factoring in computational cost, it appears that, if CCSD(T)-F12/cc-pVTZ-F12 single point calculations were not feasible, then CCSD(T)/cc-pVTZ would be the best we can do.

Considering (b), we have optimized MP2/def2-QZVP geometries and used those to assess torsion angles at the MP2 level with various basis sets. The resulting RMSD values are: cc-pVTZ 0.15, 6-31G* 0.54, 6-311G** 0.66, def2-SVP 0.82, def2-TZVP 0.48, and def2-TZVPP 0.27 degrees. MP2/cc-pVQZ geometries for a subset of species were found to be

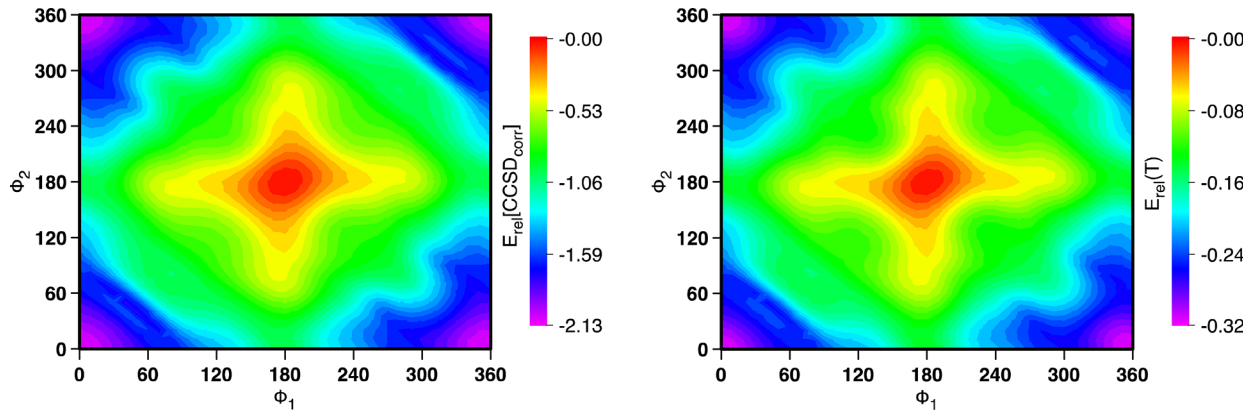


Figure 2. Contribution (kcal/mol) of CCSD correlation energy and (T) connected triple excitations to relative energies on the *n*-pentane conformer surface.

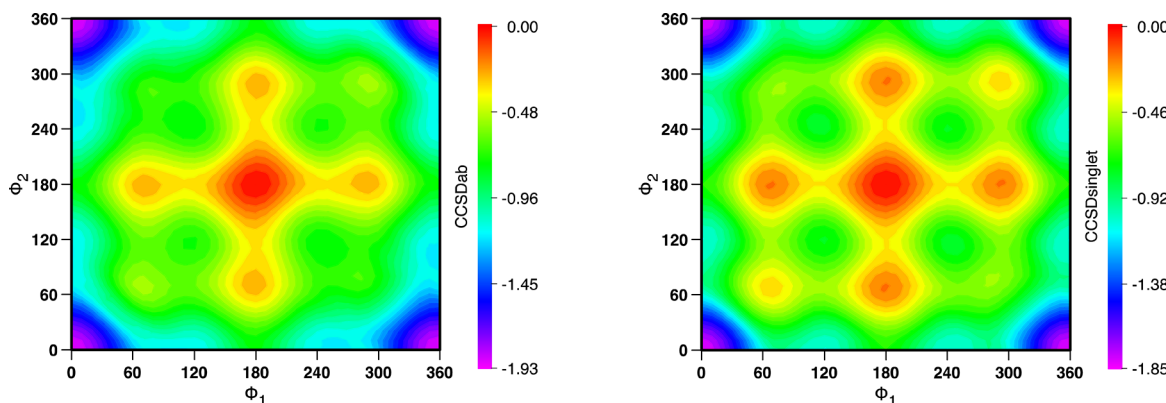


Figure 3. Opposite-spin and singlet-pair parts of the CCSD correlation contribution to relative energies (kcal/mol).

functionally equivalent to the MP2/def2-QZVP counterparts. It thus appears that, at least for the backbone torsion angles, the electron correlation method viz. DFT functional/dispersion combination has a much greater influence than the basis set.

3.2. Mapping of Conformational Surface. In light of the results in the previous section, we settled on SCS-MP2/cc-pVTZ as the level of theory for the constrained optimizations. For each point, the two backbone torsion angles were fixed and a constrained optimization carried out on the remaining internal coordinates. The torsion angles ϕ_1 and ϕ_2 were stepped in 10 degree increments, and only symmetry-unique points were considered. Considering that $E(\phi_1, \phi_2) = E(\phi_2, \phi_1)$ and $E(\phi_1, \phi_2) = E(360^\circ - \phi_1, 360^\circ - \phi_2)$, this leaves us with 343 unique points.

For these geometries (given in the SI), we carried out single-point energy calculations at the following levels: conventional CCSD(T)/cc-pVTZ (yielding MP2, SCS-MP2, MP3, SCS-MP3, MP4(SDQ), and CCSD as byproduct) and explicitly correlated CCSD(T)-F12/cc-pVDZ-F12, CCSD(T)-F12/cc-pVTZ-F12 (yielding MP2-F12/cc-pVTZ-F12 as a byproduct), and MP2-F12/cc-pVQZ-F12. (As in the previous section, the cc-pVnZ-F12 basis sets and matching density fitting basis sets were taken from refs.⁷³ and,⁷⁴ respectively, while the geminal beta values recommended in ref.⁷³ were employed. Total and relative energies are given in the SI.) The RMS difference between the CCSD(T)-F12b/cc-pVDZ-F12 and cc-pVTZ-F12 surfaces is just 0.006 kcal/mol, while the largest difference of 0.018 kcal/mol is seen at the (80,80) point; in general, the largest such differences are seen on or near the ($x, \pm x$) seams.

As an additional check for adequate basis set convergence, we considered MP2-F12/cc-pVTZ-F12 and MP2-F12/cc-pVQZ-F12 surfaces: their RMS difference is just 0.0015 kcal/mol, with a maximum of just 0.004 kcal/mol at the (30,30) point. We believe we have thus established that our explicitly correlated surface is adequately converged in the 1-particle basis set for at least the valence correlation part.

How do these surfaces compare to the conventional CCSD(T)/cc-pVTZ surface? The RMS difference between the CCSD(T)/cc-pVTZ and CCSD(T)-F12/cc-pVTZ-F12 surfaces is 0.04 kcal/mol, with a maximum of 0.105 kcal/mol at the (40,40) point. It thus appears that even the relatively inexpensive CCSD(T)-F12/cc-pVDZ-F12 approach is to be preferred over the CCSD(T)/cc-pVTZ surface, which is a useful finding for conformational energetics on larger species.

For a representative sample of structures, we considered core-valence correlation at the CCSD(T)-F12/cc-pCVDZ-F12 and CCSD(T)-F12/cc-pCVTZ-F12 levels,⁷⁵ and found these to be quite small but inadequately converged with the cc-pCVDZ-F12 basis set. In light of the already formidable computational expense for the valence surface, we have therefore refrained from carrying out any core-valence calculations on the entire surface.

Let us now consider the surface at lower *ab initio* levels of theory. First of all, even at the SCF level all minima and transition states are present and indeed a contour plot looks very similar (Figure S-2 in the SI), except that the scale would indicate “extrusion” by about 20%. In Figure 2 we see contour plots of the CCSD correlation contribution (left-hand pane)

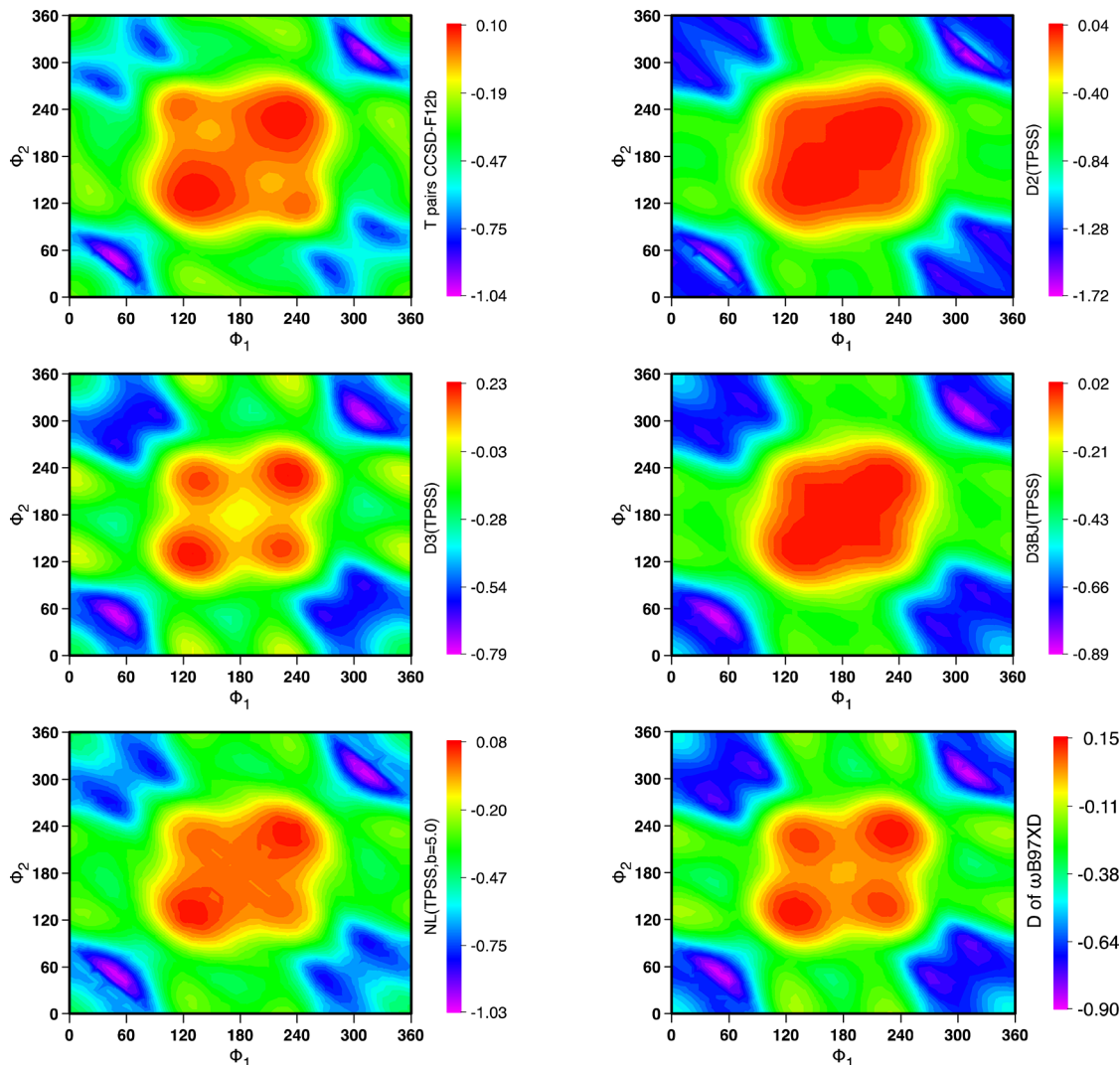


Figure 4. Triplet-pair CCSD correlation contribution to relative energies (kcal/mol) compared with five different empirical dispersion corrections.

and of the (T) triples. Qualitatively, the two plots look very similar, except that the (T) plot's energy scale is about 1/7 that of the CCSD plot. On the whole, electron correlation is seen to favor the most-strained structures.

Now let us decompose the CCSD correlation energy into opposite-spin and same-spin components, or alternatively into singlet-coupled and triplet-couplet pair components. These two decompositions are (for closed-shell systems) related by $E_{\text{CCSD}}^S = E_{ab} - (E_{aa} + E_{bb})/2 = E_{ab} - E_{ss}/2$ and $E_{\text{CCSD}}^T = 3(E_{aa} + E_{bb})/2 = (3/2)E_{ss}$. As shown in the left-hand and right-hand panes of Figure 3, opposite spin stabilizes most near the $\tau\tau$ global maximum and the $\tau\xi$ saddle points, also significantly near the $\tau\tau$ transition states and $\xi\xi^\pm$ saddle point, furthermore near gg and gx⁻ minima, least at tg. Considering the singlet-coupled (S) pairs instead, we see the same basic trends but with additional sharpness, “as if a lens had been wiped clean” (Figure 3).

As we can see in Figure 4 (top left pane), however, the triplet-coupled (T) pairs (identical to the same-spin contribution except for the 3/2 prefactor) look qualitatively very different. Here we see a mountain “mesa” around the four $\xi\xi^\pm$ structures with tt in the middle, with the greatest stabilization around the gg structures, followed by gx⁻ and then the $\gamma\gamma^-$ barrier. tg is not getting so much stabilization: visually, while both S and T surfaces have 2-fold rotational symmetry by

construction, the S surface could be described as having 4-fold ‘quasisymmetry’ while this is emphatically not true for the T surface.

The most revealing comparison, however, is with the surfaces of empirical dispersion corrections as plotted in the top-right and bottom-right panes of Figure 4. Note that, except for a flatter mesa and the gx⁻ maxima jutting out to the edge of the plot, the D2 correction displays all the ‘cartographic’ features of the T surface, except for being scaled by about 1.7. While the D3BJ correction has more sophisticated atomic Lennard-Jones parameters, a different damping function, and R^{-8} terms not present in the R^{-6} -only D2 correction, the same qualitative features are seen there but now on a similar scale as the T surface. The D3 (also known as D3zero) correction⁶² (middle left-hand pane), which has inordinately large R^{-8} contributions, has been deprecated by the Grimme group in favor of D3BJ (middle right-hand pane): as can be seen in Figure 4, its plot exhibits additional ‘terrain’, which is even more pronounced with parameters for other functionals like B3LYP. We note that the Chai–Head–Gordon correction from the ω B97X-D functional (bottom right-hand pane) looks qualitatively very similar to D3zero despite different coefficients and the complete absence of R^{-8} terms: this illustrates the importance of the damping function (which is the same as for D3zero).

We also considered the “nonlocal” Vydrov-van Voorhis van der Waals functional correction,⁶⁵ as previously benchmarked in ref 76 and implemented in ORCA 2.9.⁶⁶ The b parameters for various functionals were taken from ref 77. As can be seen in Figure 4, this correction is qualitatively much closer to D3BJ (and to the CCSD T pairs contribution) than to D3, with D2 somewhere in the middle.

The correlation matrix between the different corrections is given below:

	D2	D3	D3BJ	VV10/NL	S pairs	T pairs
D2	1.000					
D3	0.839	1.000				
D3BJ	0.977	0.817	1.000			
VV10	0.972	0.902	0.979	1.000		
S pairs	0.566	0.049	0.567	0.420	1.000	
T pairs	0.917	0.898	0.905	0.962	0.279	1.000

What about quasiperturbative triple excitations, that is, the CCSD(T)–CCSD difference? As seen in Figure 2, their contribution is fairly significant, and qualitatively resembles the CCSD correlation energy. Hence scaling the CCSD correlation energy or SCS-CCSD (parameters³⁵ $C_S = 1.27$, $C_T = 1.1766$) should be a very good approximation to the (T) contributions, and as can be seen in the SI (Figures S-3 and S-4) and in Table 4, this is indeed the case, with RMSD=0.10 kcal/mol overall

Table 4. RMSD (kcal/mol) of Wavefunction *ab initio* Methods Relative to CCSD(T) Reference Data for the *n*-Pentane Surface^a

Basis set: cc-pVTZ			Basis set: def2-QZVPP		
Ref.: CCSD(T)/cc-pVTZ reference energies			Ref.: CCSD(T)-F12/cc-pVTZ-F12		
Equal weights for all points					
HF	1.274	SCS(MI)MP2	0.568	HF	1.263
MP2	0.191	MP4(SDQ)	0.139	MP2	0.179
MP3	0.167	MP4	0.020	MP3	0.161
SCS-MP2	0.210	CCSD	0.163	SCS-MP2	0.190
SCS-MP3	0.210	SCS-CCSD	0.102	SCS-MP3	0.193
MP2.5	0.171	SCS(MI)CCSD	0.022	MP2.5	0.161
Boltzmann-weighted (T=1000 K)					
HF	0.931	SCS(MI)MP2	0.321	HF	0.913
MP2	0.091	MP4(SDQ)	0.098	MP2	0.087
MP3	0.125	MP4	0.022	MP3	0.117
SCS-MP2	0.135	CCSD	0.118	SCS-MP2	0.117
SCS-MP3	0.153	SCS-CCSD	0.066	SCS-MP3	0.138
MP2.5	0.092	SCS(MI)CCSD	0.023	MP2.5	0.083

^aSCS-MP2/cc-pVTZ reference geometries were used throughout.

and 0.066 kcal/mol in the lower regions (see below): in fact, performance of SCS(MI)CCSD⁷⁸ (with $C_S = 1.11$ and $C_T = 1.2233$) is almost too good to be true, at RMSD = 0.022 kcal/mol overall.

Perhaps a look at the paradigmatic dispersion interaction, namely the helium dimer, might be instructive here. In this system, if we decompose the interaction energy in pair energies, $\Delta E_{CCSD}^T = E[\sigma_g \sigma_u]^T$ while $\Delta E_{CCSD}^S = E[\sigma_g \sigma_g]^S + E[\sigma_u \sigma_u]^S + E[\sigma_g \sigma_u]^S - 2E[1s(\text{He})]$. As can be seen in Figure 5, energy plots versus $(r_e/r)^6$ exhibit linearity over the 0–1.4 range (and approximate linearity well beyond that) for the correlation contributions: the T pairs:S pairs:(T) triples contributions are in roughly 10:2.3:1 size ratios.

Coming back to pentane, Table 4 lists performance statistics for various wave function *ab initio* methods, both using the cc-pVTZ basis set relative to CCSD(T)/cc-pVTZ reference data, and using the def2-QZVPP basis set relative to CCSD(T)-F12/cc-pVTZ-F12 reference data. We list performance statistics

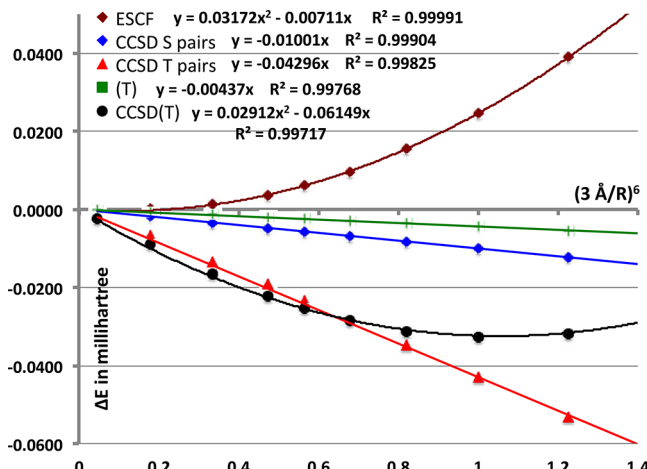


Figure 5. Breakdown of contributions (hartree) to the CCSD(T)/aug-cc-pVQZ interaction energy of He_2 .

both using equal weights, and using Boltzmann weights with a Boltzmann temperature of 1000 K. The latter statistics reduce the influence of large errors for the regions near the saddle points and especially the global maximum, and may shed additional light on performance.

Let us now break down contributions for pentane by order of perturbation theory. First of all, aside from (T) at fourth order, all the “action” is seen at second and third order. The MP2 T pairs are essentially the CCSD T pairs multiplied by 1.17, with MP3 counteracting the ‘exaggeration’ and fourth and higher order contributions quite small. The MP2 S pairs blur some structural features seen on the CCSD S pairs surface: these then reenter at third order, with the fourth and higher-order contributions again quite modest. Likewise, fifth-order (T) terms are quite trifling. (We note in Table 4 that RMSD only sees a modest drop from MP3 to MP4(SDQ), and that full MP4 has an RMSD from CCSD(T) of just 0.020 kcal/mol.) Contour plots for all of these can be found in the SI (Figures S-5 through S-10).

The error in the straight MP2 surface (Figure S-11 in the SI) varies from +0.12 kcal/mol near gg via about −0.3 kcal/mol at $\xi\xi^\pm$ and $\tau\xi^\pm$ geometries to −0.61 kcal/mol at the $\tau\tau$ global maximum. Its error is greatest in the upper reaches of the surface, as expected: RMSD drops from 0.19 kcal/mol with unit weighting to 0.09 kcal/mol with Boltzmann weighting ($T_B = 1000$ K), and to just 0.042 kcal/mol using $T_B = 298.15$ K. As to the minima, the main problem is a bias against the gg structure. SCS-MP2 does not really improve the energetics over MP2 (Figure S-12 in the SI), although it does appear to help with the geometries of the minima (see above). SCS(MI)MP2,⁷⁹ which was parametrized for weak interactions, in fact does more harm than good, RMSD increasing to 0.568 from the straight MP2 value of 0.191 kcal/mol (see also Figure S-13 in the SI). For this problem, SCS-MP3 does not offer any real improvement over SCS-MP2 (Figure S-14, SI). MP2.5,^{36,80} on the other hand (being an average of MP2 and MP3) performs excellently near minima, and fairly well near transition states: its only large errors are near the eclipsed geometries (Figure S-15, SI). The RMSDs, however, are not significantly better than those of MP2.

3.3. Performance of Density Functional Methods.

Figures 6 and 7 show error surfaces for a number of representative DFT functionals. LDA (Figure 6, bottom right-

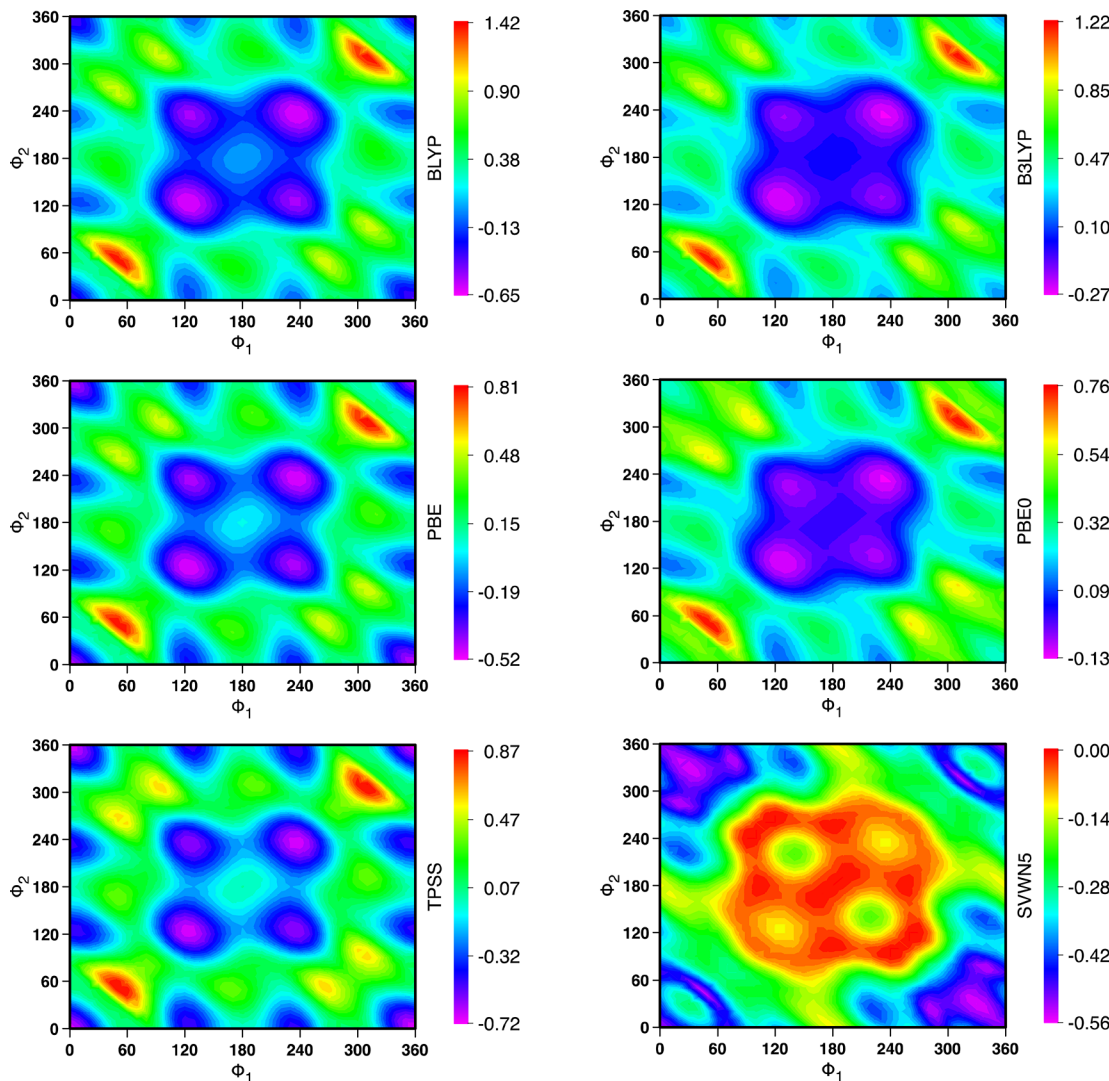


Figure 6. Error in computed conformer surfaces with some representative DFT exchange-correlation functionals (kcal/mol).

hand pane) actually over stabilizes, especially near the $\pi\pi$ and gx^- areas. This is presumably related to the well-known tendency (see, e.g., ref 81) of LDA to overestimate correlation (as it underestimates exchange). Yet for the problem at hand, LDA's error scale (0 to -0.56 kcal/mol) is actually just over one-fourth that of BLYP (+1.42 to -0.65 kcal/mol) and about three-eights that of B3LYP (+1.22 to -0.27 kcal/mol).

The error surfaces of the BLYP, BP86 (not shown), and PBE GGAs, and even of the TPSS meta-GGA, all look qualitatively quite similar, with areas of overstabilization near the second-order saddle points in general, and four deep troughs around $\xi\xi^\pm$ in particular. These troughs, in the event, are complementary to the four peaks in the D3 surface (Figure 4, middle left pane), which explains why D3 actually outperforms D3BJ for these GGAs (see Table 5 below). As can be seen for B3LYP and PBE0 in Figure 6, admixture of Hartree–Fock exchange primarily has the effect of mitigating or reversing the overstabilization around the second-order saddle points, in particular “flattening” the central area considerably: the same observation can be made for other hybrids not shown here such as B3P86, B3PW91, and TPSS0. The error range is only slightly reduced at the top but quite considerably at the bottom, e.g. from $[-0.52, 0.81]$ for PBE to $[-0.13, 0.76]$ for

PBE0. We also note that the PBE0 error surface has a very similar shape to the B3LYP one, but is scaled down considerably.

Error surfaces for additional functionals can be found in Figure S-16 of the SI. The M06 and M06–2X “implicit dispersion” functionals do span smaller error ranges, but exhibit spurious gg and gx^- stabilizations of 0.4–0.5 kcal/mol as well as erratic surfaces. GKM reported earlier that M06 actually inverts the energetic ordering of the gg and gx^- conformers.

Let us now turn to the double hybrids. B2GP-PLYP without dispersion correction (Figure 7, upper left pane) does a better job than B3LYP, but this is a low hurdle to pass. B2GP-PLYP-D2 (upper right pane) overcorrects near gg but is otherwise an improvement, while B2GP-PLYP-D3BJ (lower right pane) yields an excellent performance in the conformationally important region. The spin-component-scaled double hybrids DSD-BLYP and especially DSD-PBEP86 do quite well. Contour plots for both DSD-PBEP86-D2 and DSD-PBEP86-D3BJ varieties can be seen in Figure 8: it is seen that performance compared to SCS(MI)CCSD can be reached. Finally, contour plots for some additional SCS double hybrids can be found in the SI as Figure S-17.

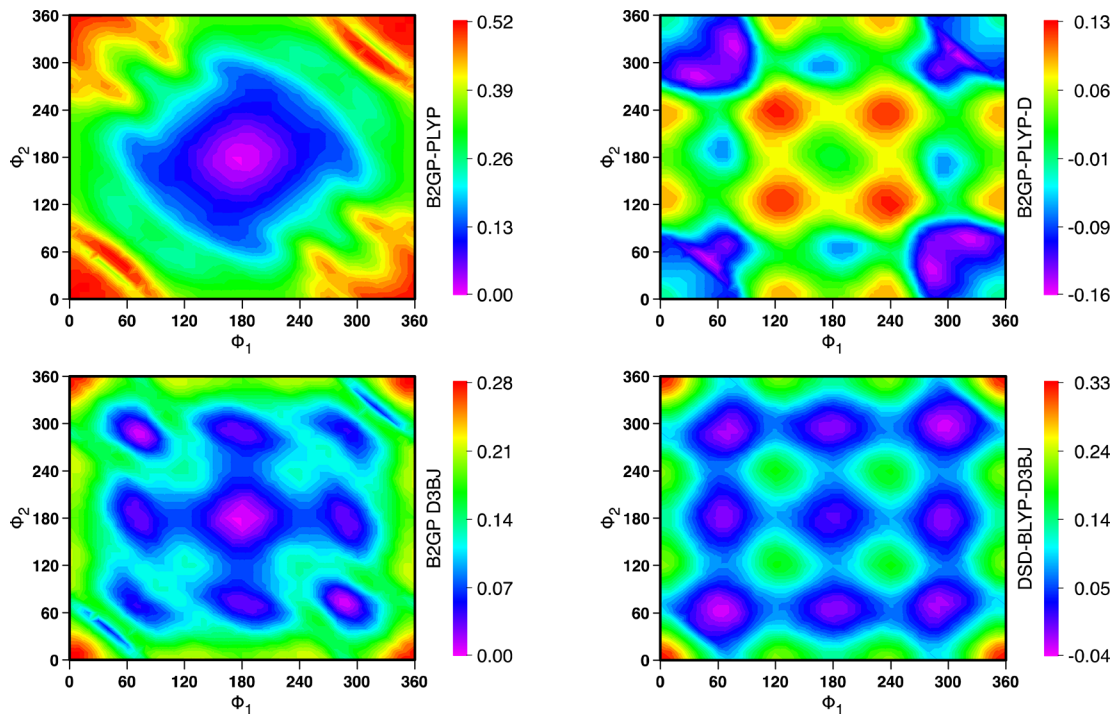


Figure 7. Error (kcal/mol) in computed conformer surfaces using the B2GP-PLYP and DSD-PLYP double hybrid functionals with and without empirical dispersion corrections.

Table 5. RMS Deviations (kcal/mol) from the CCSD(T)-F12b/cc-pVTZ-F12 Reference Surface for a Variety of Electronic Structure Methods with the cc-pVTZ Basis Set. Values Given are Raw (no D), with Various Empirical Dispersion Corrections (D2, D3, D3BJ), and using the VV10 Dispersion Model (NL). The def2-QZVPP Basis Set was Used Throughout^a

	Double hybrids			Hybrids								“pure” DFT functionals				
	DSD-PBE P86	DSD-PBEh B95	DSD-PBE B95	PWP B95	B2GP		PW6 B95		B3LYP	B3PW91	PBEO	TPSSO	TPSS	PBE	BLYP	BP86
					M06											
unweighted																
no D	0.198	0.093	0.226	0.081	0.303	0.195	0.115	0.426	0.418	0.304	0.303	0.308	0.243	0.413	0.300	
D2	0.067	0.169	0.123		0.074	0.386	0.416	0.488	0.529	0.214	0.447	0.822	0.565	0.749	0.748	
D3BJ	0.079	0.078	0.028	0.139	0.127		0.218	0.174	0.215	0.074	0.178	0.479	0.317	0.419	0.475	
NL						0.204	0.089	0.102	0.045	0.129	0.440	0.284	0.318			
D3					0.072	0.180	0.304	0.106	0.166	0.104	0.100	0.048	0.314	0.228	0.157	0.218
Boltzmann-weighted (T=1000 K)																
no D	0.134	0.061	0.163	0.075	0.238	0.188	0.100	0.437	0.418	0.296	0.313	0.293	0.259	0.462	0.327	
D2	0.062	0.148	0.100		0.067	0.352	0.288	0.315	0.364	0.133	0.298	0.508	0.337	0.448	0.472	
D3BJ	0.044	0.082	0.018	0.087	0.086		0.122	0.095	0.125	0.052	0.093	0.251	0.165	0.224	0.267	
NL						0.124	0.063	0.058	0.047	0.069	0.239	0.149	0.171			
D3					0.070	0.176	0.276	0.079	0.143	0.083	0.090	0.051	0.149	0.122	0.101	0.115

Additional functionals:

	B3P86	B3P86-NL	M06-2X	wB97X	wB97XD	M06L	M11	SVWN5
unweighted	0.317	0.117	0.132	0.069	0.168	0.432	0.486	0.280
Boltzmann	0.327	0.066	0.119	0.067	0.111	0.303	0.384	0.207

^aWeighted RMSDs use Boltzmann weights $\exp(-c_2 \Delta E / T_B)$, for a semi-arbitrary Boltzmann temperature $T_B = 1000$ K.

Can we come up with *ad hoc* spin component scaled MP2 methods? We can perform multivariate least-squares fitting over the data points. Complete neglect of same-spin MP2, that is, an *ad hoc* SOS-MP2, yields an optimized $c_{2ab} = 1.587$, which corresponds to an RMSD of just 0.030 kcal/mol. By admitting same-spin correlation as well, this can be lowered further to 0.017 kcal/mol, with $c_{2ab} = 1.517$ and $c_{2ss} = 0.184$. Admitting third-order correlation as well, this can be brought down to just

0.0044 kcal/mol, with $c_{2ab} = 1.254$, $c_{2ss} = 1.003$, and $c_3 = 0.808$. Further decomposition of c_3 into c_{3ab} and c_{3ss} does not perceptibly (let alone statistically significantly) reduce RMSD, nor does the inclusion of a constant in the fit.

While the customized SCS-MP3 may be more a curiosum than anything else, the *ad hoc* SCS-MP2 can be combined with analytical first and second derivative implementations to enable rapid optimizations and frequency calculations.

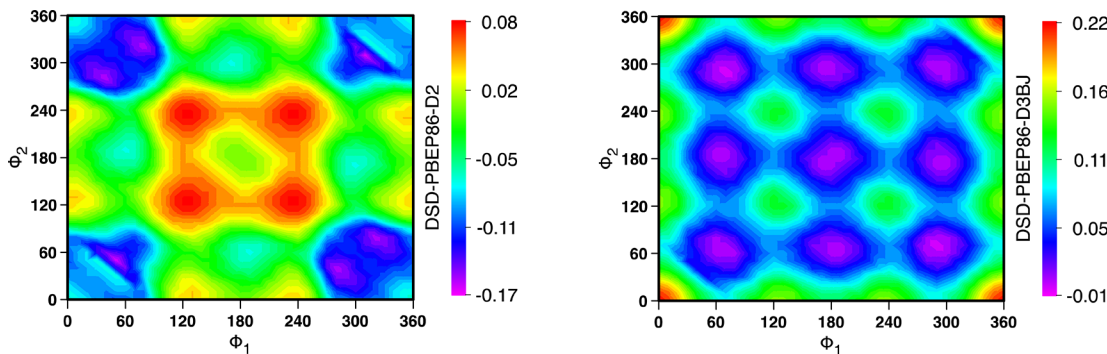


Figure 8. Error (kcal/mol) in computed conformer surfaces using the DSD-PBEP86 functional in the no-dispersion and D2 parametrizations.

Table 5 considers the performance of various DFT methods for the *n*-pentane surface, both over the whole energy spectrum and weighted toward the lower-energy region. Not surprisingly, conventional DFT functionals have a hard time without dispersion corrections. Using the D3BJ correction or the VV10 model, however, several hybrid GGAs achieve respectable performances, with even B3LYP-NL reaching RMSD = 0.09 kcal/mol. While there is no obvious advantage to hybrids over the underlying GGAs in the absence of empirical corrections, the hybrids have a clear edge when NL or D3BJ are added. (Except for the double hybrids, the older D2 often does more harm than good in a conformational context, consistent with what was found in ref 4.) The performance of PBE0-D3BJ and PBE0-NL, in particular, stands out, reaching RMSD = 0.07 and 0.05 kcal/mol, respectively (both 0.05 kcal/mol using Boltzmann weights with $T_B = 1000$ K).

Especially for the Boltzmann-weighted RMSD, PBE appears to have an edge over the other GGA (BLYP, BP86) and even over the meta-GGA (TPSS). For reasons explained above, the older D3zero correction outperforms D3BJ (and in fact even NL) for the “pure DFT” functionals: for the hybrids, either D3BJ has the edge over D3zero, or both corrections have very low RMSDs.

Among the “implicitly dispersion-corrected” functionals of the Truhlar group, the older PW6B95 actually slightly outperforms the newer M06-2X, and both have a substantial edge over M06. For PW6B95, D3 markedly outperforms D3BJ, which is probably related to the fact that both PW6B95 (and its “ancestor” B1B95⁸¹) have uncorrected error profiles (see Figure S-16, SI) qualitatively similar to those seen for the (meta)GGAs above rather than to those seen for the corresponding hybrids (compare Figures 6 and S-16, SI).

The performance of the ω B97X range-separated hybrid can only be described as stunning (see also Figure S-16, SI): in fact, ω B97X-D, which includes a dispersion correction and was globally reparametrized in its presence, surprisingly performs worse unweighted, although the gap is largely closed for the weighted RMSD. (In an attempt to see whether the performances of ω B97X and ω B97X-D are specific to this system, we considered the 12 lowest conformer energies of melatonin¹² with these functionals and the def2-QZVP basis set. The RMSDs we obtained were 0.43 kcal/mol for ω B97X and 0.33 kcal/mol for ω B97X-D: the former number is among the best for uncorrected functionals below rung five, while the latter is intermediate between D2- and D3BJ-corrected versions of common hybrid DFT functionals like PBE0. Over the entire set of 52 conformers, RMSD for ω B97X deteriorates

to 0.81 kcal/mol, while that for ω B97X-D stays essentially unchanged at 0.31 kcal/mol.)

In the process of revising this manuscript, we also considered the very recent M11 range-separated hybrid⁴¹ using the most recent release of GAMESS-US.⁸² Both the unweighted and Boltzmann-weighted RMSDs are around 0.4 kcal/mol, markedly worse than the ω B97X and ω B97X-D range-separated hybrids. We again considered the melatonin conformer set as a secondary check, and found likewise rather poor values of 0.67 kcal/mol for the lowest 12 conformer energies, and 0.77 kcal/mol for the entire set.

Among double hybrids (see also Figures 7, 8, and S-17, SI), the best performances in the absence of an empirical correction are put in by DSD-PBEB95-noD and the similar PWPB95.²⁴ (While PWPB95 uses PW91 exchange and Becke95 correlation with custom-adjusted parameters and an opposite-spin-only MP2-like term, DSD-PBEB95 leaves the underlying exchange and correlation functionals unmodified but admits a small fraction of same-spin correlation.) Using the older D2 correction, B2GP-PLYP-D in fact does best (RMSD = 0.07 kcal/mol), while with the newer D3BJ correction, the performance of DSD-PBEPBE-D3BJ is essentially too good to be true (RMSD = 0.03 kcal/mol, dropping to 0.02 with Boltzmann weighting). Yet both DSD-PBEP86-D3BJ and DSD-PBEB95-D3BJ still put in creditable performances at RMSD = 0.08 kcal/mol, which for DSD-PBEP86-D3BJ improves to 0.044 kcal/mol when Boltzmann weighting ($T_B = 1000$ K) is applied.

In the melatonin study,¹² the performance of DFT methods exhibited a number of trends that parallel the present findings. The main difference is that there, internal weak hydrogen bonds cause enough basis set dependence even at the DFT level that performance difference can be masked by basis set incompleteness if one is not careful. In contrast, in an earlier draft of the present manuscript we obtained fundamentally the same error statistics for the DFT functionals with the cc-pVTZ basis set—which is not only considerably smaller than the def2-QZVP used in Table 5 but rather suboptimal for DFT calculations as well.

4. CONCLUSIONS

In the earlier work of GKM,⁴ it was shown that conformer energies in alkanes (and other systems) are highly dispersion-driven, and that uncorrected DFT functionals fail badly at reproducing them, while simple empirical dispersion corrections tend to overcorrect. In order to gain greater insight into the nature of the phenomenon, we have mapped the torsional surface of *n*-pentane to 10-degree resolution at the CCSD(T)-

F12 level near the basis set limit. The data obtained have been decomposed by order of perturbation theory, excitation level, and same-spin vs opposite-spin character. A large number of approximate electronic structure methods have been considered, as well as several empirical dispersion corrections. Our chief conclusions are as follows: (a) the effect of dispersion is dominated by same-spin correlation (or triplet-pair correlation, from a different perspective); (b) singlet-pair correlation is important for the surface, but qualitatively very dissimilar to the dispersion component; (c) single and double excitations beyond third order are essentially unimportant for this surface; (d) connected triple excitations do play a role but are statistically very similar to the MP2 singlet-pair correlation; (e) the form of the damping function is crucial for good performance of empirical dispersion corrections; (f) at least in the lower-energy regions, SCS-MP2 and especially MP2.5 perform very well; and (g) novel spin-component scaled double hybrid functionals such as DSD-PBEP86-D2 acquit themselves very well for this problem.

■ ASSOCIATED CONTENT

S Supporting Information

Complete refs 27, 29, and 66; Table S-1 of the paper; Figures S-1 through S-17 of the paper; total energies for the 343 grid points in Excel format; coordinates (in Xmol/Jmol .xyz format) for the 14 CCSD(T)/cc-pVTZ stationary point geometries and for the 343 SCS-MP2/cc-pVTZ grid point geometries; SCS-MP2/cc-pVTZ harmonic frequencies of the 14 stationary points. Web-enhanced objects for Figure S-1 using Jmol can be found at <http://theochem.weizmann.ac.il/web/papers/pentane/n-pentane.html>.⁸³ This material is available free of charge via the Internet at <http://pubs.acs.org>.

■ AUTHOR INFORMATION

Corresponding Author

*E-mail: gershon@weizmann.ac.il

Present Address

Department of Organic Chemistry, Weizmann Institute of Science, 76100 Rehovot, Israel.

Notes

The authors declare no competing financial interest.

■ ACKNOWLEDGMENTS

This research was made possible by a generous grant of computer time from the Faculty of Chemistry at the Weizmann Institute of Science and by a startup grant at the University of North Texas. The author thanks Profs. Stefan Grimme, Martin Head-Gordon, and Stephen A. Cooke and Drs. Amir Karton and Sebastian Kozuch for helpful discussions, Drs. Mark A. Iron, Mark Vilensky, and David A. Hrovat for technical assistance, Drs. Fernando Clemente and Gary Trucks for assistance²⁸ with various aspects of GAUSSIAN, and Dr. Brina Brauer for editing the manuscript prior to submission.

■ DEDICATION

Dedicated to James E. Boggs, founder of the Austin Symposia on Molecular Structure, on the occasion of his 92nd birthday.

■ REFERENCES

- (1) International Union for Pure and Applied Chemistry (IUPAC), *IUPAC Compendium of Chemical Terminology*, 2nd ed. (also known as "The Gold Book"); McNaught, A.D., Wilkinson, A., Eds.; Blackwell

Scientific Publications: Oxford, 1997. XML on-line corrected version: <http://goldbook.iupac.org> (2006-present) created by Nic, M.; Jirat, J.; Kosata, B.; Jenkins, A. doi:10.1351/goldbook.

(2) IUPAC Gold Book, entry "Conformation", <http://goldbook.iupac.org/C01258.html> (accessed February 9, 2011).

(3) IUPAC Gold Book, entry "Conformer", <http://goldbook.iupac.org/C01262.html> (accessed February 9, 2011).

(4) Gruzman, D.; Karton, A.; Martin, J. M. L. Performance of *Ab Initio* and Density Functional Methods for Conformational Equilibria of C_nH_{2n+2} Alkane Isomers ($n = 4-8$). *J. Phys. Chem. A* **2009**, *113*, 11974–11983.

(5) Karton, A.; Gruzman, D.; Martin, J. M. L. Benchmark Thermochemistry of the C_nH_{2n+2} Alkane Isomers ($n = 2-8$) and Performance of DFT And Composite *Ab Initio* Methods for Dispersion-Driven Isomeric Equilibria. *J. Phys. Chem. A* **2009**, *113*, 8434–8447.

(6) Bakowies, D. *Ab Initio* Thermochemistry with High-Level Isodesmic Corrections: Validation of the ATOMIC Protocol for a Large Set of Compounds with First-Row Atoms (H, C, N, O, F). *J. Phys. Chem. A* **2009**, *113*, 11517–11534.

(7) Tasi, G.; Mizukami, F. Scaled Effective One-Electron Method Based on G2 Theory: Results for Aliphatic Alkane Molecules. *J. Chem. Inf. Comput. Sci.* **1998**, *38*, 632–638.

(8) Tasi, G.; Mizukami, F.; Pálinkó, I.; Csontos, J.; Gyorffy, W.; Nair, P.; Maeda, K.; Toba, M.; Niwa, S.-I.; Kiyozumi, Y.; Kiricsi, I. Enumeration of the Conformers of Unbranched Aliphatic Alkanes. *J. Phys. Chem. A* **1998**, *102*, 7698–7703.

(9) Tasi, G.; Izsák, R.; Matisz, G.; Császár, A. G.; Kállay, M.; Ruscic, B.; Stanton, J. F. The Origin of Systematic Error in the Standard Enthalpies of Formation of Hydrocarbons Computed via Atomization Schemes. *ChemPhysChem* **2006**, *7*, 1664–1667.

(10) See, e.g.; McGaughey, G. B.; Sheridan, R. P.; Bayly, C. I.; Culberson, J. C.; Kreatsoulas, C.; Lindsley, S.; Maiorov, V.; Truchon, J.-F.; Cornell, W. D. Comparison Of Topological, Shape, And Docking Methods In Virtual Screening. *J. Chem. Inf. Model.* **2007**, *47*, 1504–1519 and references therein.

(11) Tasi, G.; Mizukami, F. Quantum Algebraic–Combinatorial Study of the Conformational Properties of n-Alkanes. I. *J. Math. Chem.* **1999**, *25*, 55–64. Tasi, G.; Mizukami, F.; Csontos, J.; Gyorffy, W.; Pálinkó, I. Quantum Algebraic–Combinatorial Study of the Conformational Properties of n-Alkanes. II. *J. Math. Chem.* **2000**, *27*, 191–199.

(12) Fogueri, U. R.; Kozuch, S.; Karton, A.; Martin, J. M. L. The Melatonin Conformer Space: Benchmark and Assessment of Wavefunction and DFT Methods for a Paradigmatic Biological and Pharmacological Molecule. *J. Phys. Chem. A* **2013**, *117*, 2269–2277.

(13) Schleyer, P. von R.; Williams, J. E.; Blanchard, K. R. Evaluation of Strain in Hydrocarbons. The Strain in Adamantane and its Origin. *J. Am. Chem. Soc.* **1970**, *92*, 2377–2386.

(14) Balabin, R. M. Enthalpy Difference between Conformations of Normal Alkanes: Raman Spectroscopy Study of n-Pentane and n-Butane. *J. Phys. Chem. A* **2009**, *113*, 1012–1019. See also Tasi, G.; Nagy, B. Comment on 'Enthalpy Difference between Conformations of Normal Alkanes: Raman Spectroscopy Study of n-Pentane and n-Butane'. *J. Phys. Chem. A* **2010**, *114*, 6728–6728. Balabin, R. M. Reply to "Comment on 'Enthalpy Difference between Conformations of Normal Alkanes: Raman Spectroscopy Study of n-Pentane and n-Butane'". *J. Phys. Chem. A* **2010**, *114*, 6729–6730. Barna, D.; Nagy, B.; Csontos, J.; Császár, A. G.; Tasi, G. Benchmarking Experimental and Computational Thermochemical Data: A Case Study of the Butane Conformers. *J. Chem. Theor. Comput.* **2012**, *8*, 479–486.

(15) Klauda, J. B.; Pastor, R. W.; Brooks, B. R. Adjacent Gauche Stabilization in Linear Alkanes: Implications for Polymer Models and Conformational Analysis. *J. Phys. Chem. B* **2005**, *109*, 15684–15686. See also Klauda, J. B.; Brooks, B. R.; MacKerell, A. D., Jr.; Venable, R. M.; Pastor, R. W. An *ab Initio* Study on the Torsional Surface of Alkanes and Its Effect on Molecular Simulations of Alkanes and a DPPC Bilayer. *J. Phys. Chem. B* **2005**, *109*, 5300–5311.

(16) Salam, A.; Deleuze, M. S. High-level theoretical study of the conformational equilibrium of n-pentane. *J. Chem. Phys.* **2002**, *116*,

- 1296–1302. Knippenberg, S.; Huang, Y. R.; Hajgató, B.; François, J.-P.; Deng, J. K.; Deleuze, M. S. Probing Molecular Conformations in Momentum Space: The Case of n-Pentane. *J. Chem. Phys.* **2007**, *127*, 174306. Morini, F.; Knippenberg, S.; Deleuze, M. S.; Hajgató, B. Quantum Chemical Study of Conformational Fingerprints in the Photoelectron Spectra and (e, 2e) Electron Momentum Distributions of n-Hexane. *J. Phys. Chem. A* **2010**, *114*, 4400–4417.
- (17) Allinger, N. L.; Fermann, J. T.; Allen, W. D.; Schaefer, H. F., III The Torsional Conformations of Butane: Definitive Energetics from *Ab Initio* Methods. *J. Chem. Phys.* **1997**, *106*, 5143–5150.
- (18) Smith, G. D.; Jaffe, R. L. Quantum Chemistry Study of Conformational Energies and Rotational Energy Barriers in n-Alkanes. *J. Phys. Chem.* **1996**, *100*, 18718–18724.
- (19) Thomas, L. L.; Christakis, T. J.; Jorgensen, W. L. Conformation of Alkanes in the Gas Phase and Pure Liquids. *J. Phys. Chem. B* **2006**, *110*, 21198–21204.
- (20) Sebak, J.; Pele, L.; Potma, E. O.; Gerber, R. B. Raman Spectra of Long Chain Hydrocarbons: Anharmonic Calculations, Experiment and Implications for Imaging of Biomembranes. *Phys. Chem. Chem. Phys.* **2011**, *13*, 12724–12733.
- (21) Koglin, E.; Meier, R. J. An Ab-Initio Study of the Relative Stability of the ggg and the gtg Conformer in Hexane. *Chem. Phys. Lett.* **1999**, *312*, 284–290.
- (22) Grimme, S. Semiempirical GGA-type Density Functional Constructed with a Long-Range Dispersion Correction. *J. Comput. Chem.* **2006**, *27*, 1787–1799.
- (23) Goerigk, L.; Grimme, S. A General Database for Main Group Thermochemistry, Kinetics, and Noncovalent Interactions – Assessment of Common and Reparameterized (meta-)GGA Density Functionals. *J. Chem. Theory Comput.* **2010**, *6*, 107–126.
- (24) Goerigk, L.; Grimme, S. Efficient and Accurate Double-Hybrid-Meta-GGA Density Functionals—Evaluation with the Extended GMTKN30 Database for General Main Group Thermochemistry, Kinetics, and Noncovalent Interactions. *J. Chem. Theory Comput.* **2011**, *7*, 291–309.
- (25) Zwier, T. S. Laser Probes of Conformational Isomerization in Flexible Molecules and Complexes. *J. Phys. Chem. A* **2006**, *110*, 4133–4150.
- (26) Tasi, G.; Nagy, B.; Matisz, G.; Tasi, T. S. Similarity Analysis of the Conformational Potential Energy Surface of n-Pentane. *Comput. Theor. Chem.* **2011**, *963*, 378–383.
- (27) Frisch, M. J.; Trucks, G. W.; Schlegel, H. B.; Scuseria, G. E.; Robb, M. A.; Cheeseman, J. R.; Scalmani, G.; Barone, V.; Mennucci, B.; Petersson, G. A.; et al., GAUSSIAN 09, Revision C.01; Gaussian, Inc.: Wallingford, CT, 2009; <http://www.gaussian.com>.
- (28) We thank Fernando R. Clemente of Gaussian, Inc. for assistance with this, and Gary W. Trucks of the same company for assistance with making the MP3 code print out like-spin and opposite-spin contributions.
- (29) MOLPRO is a package of *ab initio* programs written by Werner, H.-J.; Knowles, P. J.; Manby, F. R. Schütz, M.; Celani, P.; Knizia, G.; Korona, T.; Lindh, R.; Mitrushenkov, A.; Rauhut, G.; et al.; <http://www.molpro.net>. See also: Werner, H.-J.; Knowles, P. J.; Knizia, G.; Manby, F. R.; Schütz, M. Molpro: A General-Purpose quantum chemistry program package. *WIREs Comput. Mol. Sci.* **2012**, *2*, 242–253.
- (30) Knizia, G.; Adler, T. B.; Werner, H.-J. Simplified CCSD(T)-F12 methods: Theory and benchmarks. *J. Chem. Phys.* **2009**, *130*, 054104. Adler, T. B.; Knizia, G.; Werner, H.-J. A simple and efficient CCSD(T)-F12 approximation. *J. Chem. Phys.* **2007**, *127*, 221106.
- (31) (a) Grimme, S. Improved second-order Møller–Plesset perturbation theory by separate scaling of parallel- and antiparallel-spin pair correlation energies. *J. Chem. Phys.* **2003**, *118*, 9095–9102. For a physical interpretation of the SCS-MP2 method in terms of Feenberg scaling, see: (b) Szabados, A. Theoretical interpretation of Grimme's spin-component-scaled second order Møller–Plesset theory. *J. Chem. Phys.* **2006**, *125*, 214105. For another perspective, see Fink, R. F. Spin-Component-Scaled Møller–Plesset (SCS-MP) Perturbation Theory: A Generalization of the MP Approach with Improved Properties. *J. Chem. Phys.* **2010**, *133*, 174113.
- (32) For a review, see Grimme, S.; Goerigk, L.; Fink, R. F. Spin-Component-Scaled Electron Correlation Methods. *WIREs Comput. Mol. Sci.* **2012**, *2*, 886–906.
- (33) Jung, Y. S.; Lochan, R. C.; Dutoi, A. D.; Head-Gordon, M. Scaled Opposite-Spin Second Order Møller–Plesset Correlation Energy: An Economical Electronic Structure Method. *J. Chem. Phys.* **2004**, *121*, 9793–9802.
- (34) Grimme, S. Improved Third-Order Møller–Plesset Perturbation Theory. *J. Comput. Chem.* **2003**, *24*, 1529–1537.
- (35) Takatani, T.; Hohenstein, E. G.; Sherrill, C. D. Improvement of the Coupled-Cluster Singles and Doubles Method via Scaling Same-And Opposite-Spin Components of the Double Excitation Correlation Energy. *J. Chem. Phys.* **2008**, *128*, 124111.
- (36) Pitoňák, M.; Neogrády, P.; Černý, J.; Grimme, S.; Hobza, P. Scaled MP3 Non-Covalent Interaction Energies Agree Closely with Accurate CCSD(T) Benchmark Data. *ChemPhysChem* **2009**, *10*, 282–289.
- (37) Kümmel, S.; Kronik, L. Orbital-Dependent Density Functionals: Theory and Applications. *Rev. Mod. Phys.* **2008**, *80*, 3–60.
- (38) Peverati, R.; Truhlar, D. G. The Quest for a Universal Density Functional: The Accuracy of Density Functionals across a broad Spectrum of Databases in Chemistry and Physics, preprint (Dec. 4, 2012), <http://arxiv.org/pdf/1212.0944.pdf>.
- (39) Yanai, T.; Tew, D. P.; Handy, N. C. A New Hybrid Exchange-Correlation Functional Using The Coulomb-Attenuating Method (CAM-B3LYP). *Chem. Phys. Lett.* **2004**, *393*, 51–57.
- (40) See, e.g.; Baer, R.; Livshits, E.; Salzner, U. Tuned Range-Separated Hybrids in Density Functional Theory. *Annu. Rev. Phys. Chem.* **2010**, *61*, 85–109 for a review.
- (41) Peverati, R.; Truhlar, D. G. Improving the Accuracy of Hybrid Meta-GGA Density Functionals by Range Separation. *J. Phys. Chem. Lett.* **2011**, *2*, 2810–2817. M11-L: A Local Density Functional That Provides Improved Accuracy for Electronic Structure Calculations in Chemistry and Physics. *ibid.* **2012**, *3*, 117–124.
- (42) Heyd, J., E.g.; Scuseria, G. E.; Ernzerhof, M. Hybrid Functionals Based on a Screened Coulomb Potential. *J. Chem. Phys.* **2003**, *118*, 8207–8215; erratum **2006**, *124*, 219906. Krukau, A. V.; Vydrov, O. A.; Izmaylov, A. F.; Scuseria, G. E. Influence Of The Exchange Screening Parameter On The Performance Of Screened Hybrid Functionals. *J. Chem. Phys.* **2006**, *125*, 224106.
- (43) For reviews see: (a) Eshuis, H.; Bates, J. E.; Furche, F. Electron Correlation Methods Based On The Random Phase Approximation. *Theor. Chem. Acc.* **2012**, *131*, 1084. (b) Ren, X.; Rinke, P.; Joas, C.; Scheffler, M. Random-Phase Approximation and its Applications in Computational Chemistry and Materials Science. *J. Mater. Sci.* **2012**, *47*, 7447–7471.
- (44) Perdew, J. P.; Schmidt, K. Jacob's Ladder of Density Functional Approximations for the Exchange-correlation Energy. *AIP Conf. Proc.* **2001**, *577*, 1–20.
- (45) Becke, A. D. Density-functional Exchange-energy Approximation with Correct Asymptotic Behavior. *Phys. Rev. A* **1988**, *38*, 3098–3100. Lee, C.; Yang, W.; Parr, R. G. Development of the Colle-Salvetti Correlation-energy Formula into a Functional of the Electron Density. *Phys. Rev. B* **1988**, *37*, 785–789.
- (46) (a) Perdew, J. P.; Burke, K.; Ernzerhof, M. Generalized Gradient Approximation Made Simple. *Phys. Rev. Lett.* **1996**, *77*, 3865–3868; Erratum: (b) **1997**, *78*, 1396.
- (47) Becke, A. D. Density-functional Thermochemistry. III. The Role of Exact Exchange. *J. Chem. Phys.* **1993**, *98*, 5648–5652. This paper defines the B3 hybrid exchange functional; the first published reference to the “B3LYP” combination appears to be: Stephens, P. J.; Devlin, F. J.; Chabalowski, C. F.; Frisch, M. J. *Ab Initio* Calculation of Vibrational Absorption and Circular Dichroism Spectra Using Density Functional Force Fields. *J. Phys. Chem.* **1994**, *98*, 11623–11627.

- (48) Adamo, C.; Barone, V. Toward Reliable Density Functional Methods without Adjustable Parameters: The PBE0 Model. *J. Chem. Phys.* **1999**, *110*, 6158–6170.
- (49) (a) Zhao, Y.; Truhlar, D. G. The M06 Suite of Density Functionals for Main Group Thermochemistry, Thermochemical Kinetics, Noncovalent Interactions, Excited States, and Transition Elements: Two New Functionals and Systematic Testing of Four M06-class Functionals and 12 Other Functionals. *Theor. Chem. Acc.* **2007**, *120*, 215–241. (b) Zhao, Y.; Truhlar, D. G. Density Functionals with Broad Applicability in Chemistry. *Acc. Chem. Res.* **2008**, *41*, 157–167. See also: Zhao, Y.; Truhlar, D. G. A New Local Density Functional for Main-group Thermochemistry, Transition Metal Bonding, Thermochemical Kinetics, and Noncovalent Interactions. *J. Chem. Phys.* **2006**, *125*, 194101.
- (50) Grimme, S. Semiempirical Hybrid Density Functional with Perturbative Second-order Correlation. *J. Chem. Phys.* **2006**, *124*, 034108.
- (51) Karton, A.; Tarnopolsky, A.; Lamère, J.-F.; Schatz, G. C.; Martin, J. M. L. Highly Accurate First-Principles Benchmark Data Sets for the Parametrization and Validation of Density Functional and Other Approximate Methods. Derivation of a Robust, Generally Applicable, Double-Hybrid Functional for Thermochemistry and Thermochemical Kinetics. *J. Phys. Chem. A* **2008**, *112*, 12868–12886.
- (52) Kozuch, S.; Gruzman, D.; Martin, J. M. L. DSD-BLYP: A General Purpose Double Hybrid Density Functional Including Spin Component Scaling and Dispersion Correction. *J. Phys. Chem. C* **2010**, *114*, 20801–20808.
- (53) (a) Kozuch, S.; Martin, J. M. L. DSD-PBEP86: In Search of the Best Double-hybrid DFT with Spin-component Scaled MP2 and Dispersion Corrections. *Phys. Chem. Chem. Phys.* **2011**, *13*, 20104–20107. (b) Kozuch, S.; Martin, J. M. L. Double-hybrids: An extensive search for the best functionals that mate DFT and perturbation theory. *J. Comput. Chem.* **2013**, submitted.
- (54) Chai, J.-D.; Head-Gordon, M. Systematic Optimization of Long-range Corrected Hybrid Density Functionals. *J. Chem. Phys.* **2008**, *128*, 084106.
- (55) Chai, J.-D.; Head-Gordon, M. Long-range Corrected Hybrid Density Functionals with Damped Atom-atom Dispersion Corrections. *Phys. Chem. Chem. Phys.* **2008**, *10*, 6615–6620.
- (56) Dunning, T. H., Jr. Gaussian Basis Sets for Use in Correlated Molecular Calculations. I. The Atoms Boron through Neon and Hydrogen. *J. Chem. Phys.* **1989**, *90*, 1007–1023.
- (57) Kendall, R. A.; Dunning, T. H., Jr.; Harrison, R. J. Electron Affinities of the First-row Atoms Revisited. Systematic Basis Sets and Wave Functions. *J. Chem. Phys.* **1992**, *96*, 6796–6806.
- (58) Jensen, F. Polarization consistent basis sets: Principles. *J. Chem. Phys.* **2002**, *115*, 9113–9125. Jensen, F. Polarization consistent basis sets. II. Estimating the Kohn–Sham basis set limit. *J. Chem. Phys.* **2002**, *116*, 7372–7379.
- (59) Weigend, F.; Ahlrichs, R. Balanced Basis Sets of Split Valence, Triple Zeta Valence and Quadruple Zeta Valence Quality for H to Rn: Design and Assessment of Accuracy. *Phys. Chem. Chem. Phys.* **2005**, *7*, 3297–3305.
- (60) For a review see: Grimme, S. Density Functional Theory with London Dispersion Corrections. *WIREs Comp. Mol. Sci.* **2011**, *1*, 211–228.
- (61) Jurečka, P.; Šponer, J.; Černý, J.; Hobza, P. Benchmark Database of Accurate (MP2 and CCSD(T)) Complete Basis Set Limit) Interaction Energies of Small Model Complexes, DNA Base Pairs, and Amino Acid Pairs. *Phys. Chem. Chem. Phys.* **2006**, *8*, 1985–1993; see also <http://www.begdb.com/>
- (62) Grimme, S.; Antony, J.; Ehrlich, S.; Krieg, H. A Consistent and Accurate *Ab Initio* Parametrization of Density Functional Dispersion Correction (DFT-D) For the 94 Elements. *H-Pu. J. Chem. Phys.* **2010**, *132*, 154104.
- (63) Grimme, S.; Ehrlich, S.; Goerigk, L. Effect of the Damping Function in Dispersion Corrected Density Functional Theory. *J. Comput. Chem.* **2011**, *32*, 1456–1465.
- (64) Becke, A. D.; Johnson, E. R. Exchange-hole Dipole Moment and the Dispersion Interaction Revisited. *J. Chem. Phys.* **2005**, *122*, 154108. Johnson, E. R.; Becke, A. D. A Density-functional Model of the Dispersion Interaction. *J. Chem. Phys.* **2005**, *123*, 154101. Johnson, E. R.; Becke, A. D. A Post-Hartree-Fock Model of Intermolecular Interactions: Inclusion of Higher-order Corrections. *J. Chem. Phys.* **2006**, *124*, 174104. See also Koide, A. A New Expansion for Dispersion Forces and Its Application. *J. Phys. B* **1976**, *9*, 3173–3183.
- (65) Vydrov, O. A.; Van Voorhis, T. Nonlocal Van Der Waals Density Functional: The Simpler the Better. *J. Chem. Phys.* **2010**, *133*, 244103.
- (66) Neese, F.; Wenmohs, F. ORCA 2.9; Ruhr, M. a. d. , Ed.; Max-Planck-Institute for Bioinorganic Chemistry: Germany, 2012. With contributions from: Becker, U.; Bykov, D.; Ganyushin, D.; Hansen, A.; Izsak, R.; Liakos, D. G. ; Kollmar, C.; Kossmann, S.; Pantazis, D. A. ; Petrenko, T.; et al. and additional contributions from Kállay, M.; Grimme, S.; Valeev, E. See also: Neese, F. The ORCA Program System. *WIREs Comput. Mol. Sci.* **2011**, *2*, 73–78.
- (67) Klimeš, J.; Michaelides, A. Perspective: Advances and Challenges in Treating van der Waals Dispersion Forces in Density Functional Theory. *J. Chem. Phys.* **2012**, *137*, 120901.
- (68) See, for example: DiLabio, G. A. Accurate Treatment of van der Waals Interactions Using Standard Density Functional Theory Methods with Effective Core-type Potentials: Application to Carbon-containing Dimers. *Chem. Phys. Lett.* **2008**, *455*, 348–353.
- (69) Tkatchenko, A.; Scheffler, M. Accurate Molecular Van Der Waals Interactions from Ground-State Electron Density and Free-Atom Reference Data. *Phys. Rev. Lett.* **2009**, *102*, 073005.
- (70) Dion, M.; Rydberg, H.; Schröder, E.; Langreth, D. C.; Lundqvist, B. I. Van der Waals Density Functional for General Geometries. *Phys. Rev. Lett.* **2004**, *92*, 246401.
- (71) Lee, K.; Murray, E. D.; Kong, L.; Lundqvist, B. I.; Langreth, D. C. Higher-accuracy van der Waals Density Functional. *Phys. Rev. B* **2010**, *82*, 081101.
- (72) Marchetti, O.; Werner, H. J. Accurate Calculations of Intermolecular Interaction Energies Using Explicitly Correlated Wave Functions. *Phys. Chem. Chem. Phys.* **2008**, *10*, 3400–3409; Accurate Calculations of Intermolecular Interaction Energies Using Explicitly Correlated Coupled Cluster Wave Functions and a Dispersion-Weighted MP2 Method. *J. Phys. Chem. A* **2009**, *113*, 11580–11585 specifically eq 8 there. The issues with counterpoise calculations pointed out there are not relevant in the present case.
- (73) Peterson, K. A.; Adler, T. B.; Werner, H.-J. Systematically Convergent Basis Sets for Explicitly Correlated Wavefunctions: The Atoms H, He, B–Ne, and Al–Ar. *J. Chem. Phys.* **2008**, *128*, 084102.
- (74) Yousaf, K. E.; Peterson, K. A. Optimized Auxiliary Basis Sets for Explicitly Correlated Methods. *J. Chem. Phys.* **2008**, *129*, 184108.
- (75) Hill, J. G.; Mazumder, S.; Peterson, K. A. Correlation Consistent Basis Sets for Molecular Core-valence Effects with Explicitly Correlated Wave Functions: The Atoms B–Ne and Al–Ar. *J. Chem. Phys.* **2010**, *132*, 054108.
- (76) (a) Hujo, W.; Grimme, S. Performance of the van der Waals Density Functional VV10 and (hybrid)GGA Variants for Thermochemistry and Noncovalent Interactions. *J. Chem. Theory Comput.* **2011**, *7*, 3866–3871. (b) Hujo, W.; Grimme, S. Comparison of the Performance of Dispersion-corrected Density Functional Theory for Weak Hydrogen Bonds. *Phys. Chem. Chem. Phys.* **2011**, *13*, 13942–13950.
- (77) Hujo, W.; Grimme, S. personal communication (June 25, 2012). The parameters communicated and used in this work are: PW6B95 *b* = 9.0, TPSS 5.0, TPSS0 5.5, TPSSh 5.2, PBE0 6.9, B3P86 5.3, PW1PW 7.7 and mPW1PW91 5.3.
- (78) Pitonak, M.; Rezac, J.; Hobza, P. Spin-component Scaled Coupled-clusters Singles and Doubles Optimized towards Calculation of Noncovalent Interactions. *Phys. Chem. Chem. Phys.* **2010**, *12*, 9611–9614.
- (79) DiStasio, R. A.; Head-Gordon, M. Optimized Spin-component Scaled Second-order Moller-Plesset Perturbation Theory for Intermolecular Interaction Energies. *Mol. Phys.* **2007**, *105*, 1073–1083.

(80) Riley, K. E.; Rezac, J.; Hobza, P.; MP2., X. A Generalized MP2.5 Method That Produces Improved Binding Energies with Smaller Basis Sets. *Phys. Chem. Chem. Phys.* **2011**, *13*, 21121–21125. and references therein; Sedlak, R.; Riley, K. E.; Řezáč, J.; Pitoňák, M.; Hobza, P. MP2.5 and MP2.X: Approaching CCSD(T) Quality Description of Noncovalent Interaction at the Cost of a Single CCSD Iteration. *ChemPhysChem* **2013**, *14*, 698–707.

(81) Becke, A. D. Density functional thermochemistry. IV. A new dynamical correlation functional and implications for exact exchange mixing. *J. Chem. Phys.* **1996**, *104*, 1040–1046.

(82) Schmidt, M. W.; Baldridge, K. K.; Boatz, J. A.; Elbert, S. T.; Gordon, M. S.; Jensen, J. H.; Koseki, S.; Matsunaga, N.; Nguyen, K. A.; Su, S.; Windus, T. L.; Dupuis, M.; Montgomery, J. A. General Atomic and Molecular Electronic Structure System (GAMESS). *J. Comput. Chem.* **1993**, *14*, 1347–1363 See also <http://www.msg.ameslab.gov/gamess/>.

(83) Hanson, R. M. Jmol - A Paradigm Shift in Crystallographic Visualization. *J. Appl. Crystallogr.* **2010**, *43*, 1250–1260 and references therein. See also <http://jmol.sourceforge.net>.